Protein Folding and Assembly

Deutsche Ausgabe: DOI: 10.1002/ange.201507728
Internationale Ausgabe: DOI: 10.1002/anie.201507728

Asymmetric Modulation of Protein Order–Disorder Transitions by Phosphorylation and Partner Binding

Priya R. Banerjee, Diana M. Mitrea, Richard W. Kriwacki, and Ashok A. Deniz**

Abstract: *As for many intrinsically disordered proteins, order–disorder transitions in the N-terminal oligomerization domain of the multifunctional nucleolar protein nucleophosmin (Npm-N) are central to its function, with phosphorylation and partner binding acting as regulatory switches. However, the mechanism of this transition and its regulation remain poorly understood. In this study, single-molecule and ensemble experiments revealed pathways with alternative sequences of folding and assembly steps for Npm-N. Pathways could be switched by altering the ionic strength. Phosphorylation resulted in pathway-specific effects, and decoupled folding and assembly steps to facilitate disorder. Conversely, binding to a physiological partner locked Npm-N in ordered pentamers and counteracted the effects of phosphorylation. The mechanistic plasticity found in the Npm-N order–disorder transition enabled a complex interplay of phosphorylation and partner-binding steps to modulate its folding landscape.*

Many intrinsically disordered proteins (IDPs) experience function-altering transitions between ordered and disordered states.[1] These transitions can be triggered by post-translational modifications (PTMs), such as phosphorylation,[1b] and binding partners.[2] Although recent studies have demonstrated the effects of phosphorylation and ligand association on the conformation of some polymorphic IDPs,[1b,3] detailed mechanistic descriptions of the transition pathways between ordered and disordered states, and how they are modulated by these function-altering triggers, are generally lacking. In this study, we investigated the folding landscape of the N-terminal oligomerization domain (Npm-N) of nucleophosmin (NPM1). NPM1 is a nucleolar phosphoprotein with key roles in ribosome biogenesis, centrosome duplication, p53-dependent and p53-independent tumor-suppression pathways, apoptosis, and cancer.[4] Npm-N interconverts between a globally disordered monomer and an ordered β-sheet-rich pentamer. This conformational equilibrium can be tuned by altering the ionic strength of the solution in vitro.[1b,5] Importantly, the structural polymorphism of Npm-N has been proposed to be a key factor for the multifunctionality of NPM1, and is regulated by phosphorylation and partner binding.[1b] The folded oligomeric form is required for nucleolar localization of NPM1.[6] Strikingly, phosphorylation of a single buried residue in Npm-N, Ser48, by AKT kinase prevents NPM1 oligomerization, thus causing the relocalization of NPM1 and its nucleolar binding partner Arf into the nucleoplasm and activation of the p53 tumor suppressor.[7] However, the molecular mechanism of the order (pentamer)–disorder (monomer) transition of Npm-N remains poorly understood.

To study this mechanism, we first used ensemble circular dichroism (CD) and Förster (fluorescence) resonance energy transfer (FRET) experiments to measure the reaction kinetics, by utilizing a change from low to high salt concentration (7.5 to 150 mM) as a trigger for the formation of the folded pentamer (F_P) from the disordered monomer (U_M). The CD measurements reported on secondary-structure formation (folding, Figure 1a; see also Figures 1a,c in the Supporting Information). Given that FRET between protein monomers labeled with either a donor or an acceptor dye can occur only following assembly, ensemble intermolecular FRET provided information about the assembly kinetics (Figure 1a; see also Figure 1b,d in the Supporting Information). At the high salt concentration and a 10 μM concentration of Npm-N, we observed that both folding and assembly kinetics were slow, with folding (Figure 1b; $\tau_F = (1167 \pm 7)$ s) being faster than assembly (Figure 1b; $\tau_A^{obs} = (1711 \pm 11)$ s). Furthermore, the folding time constant was observed to be independent of the Npm-N concentration, whereas the assembly time constant decreased monotonically at lower Npm-N concentrations and plateaued at a value similar to τ_F at higher concentrations (Figure 1c; concentration range: 2–25 μM). Together these data indicated that in this transition pathway, the monomer-folding step occurs prior to assembly.

Next, we used single-molecule FRET (smFRET) experiments on freely diffusing molecules to further study the transition pathway[8] by monitoring intramolecular (folding) conformational changes during the reaction. For these experiments, we developed an orthogonal labeling scheme (see Note 1 in the Supporting Information for details) by using a combination of known reactions to site-specifically label Npm-N with a FRET dye pair at positions 1 and 104 (termed Npm-N 1*/104). First, we modified the N-terminus of Npm-N to introduce a ketone functional group by the use of pyridoxal-5′-phosphate (PLP),[9] followed by labeling with

[*] P. R. Banerjee, A. A. Deniz
Department of Integrative Structural and Computational Biology
The Scripps Research Institute
La Jolla, CA 92307 (USA)
E-mail: deniz@scripps.edu
D. M. Mitrea, R. W. Kriwacki
Department of Structural Biology
St. Jude Children's Research Hospital
Memphis, TN 38105 (USA)
E-mail: richard.kriwacki@stjude.org
R. W. Kriwacki
Department of Microbiology, Immunology and Biochemistry
University of Tennessee Health Sciences Center
Memphis, TN 38163 (USA)

Supporting information for this article is available on the WWW under http://dx.doi.org/10.1002/anie.201507728.

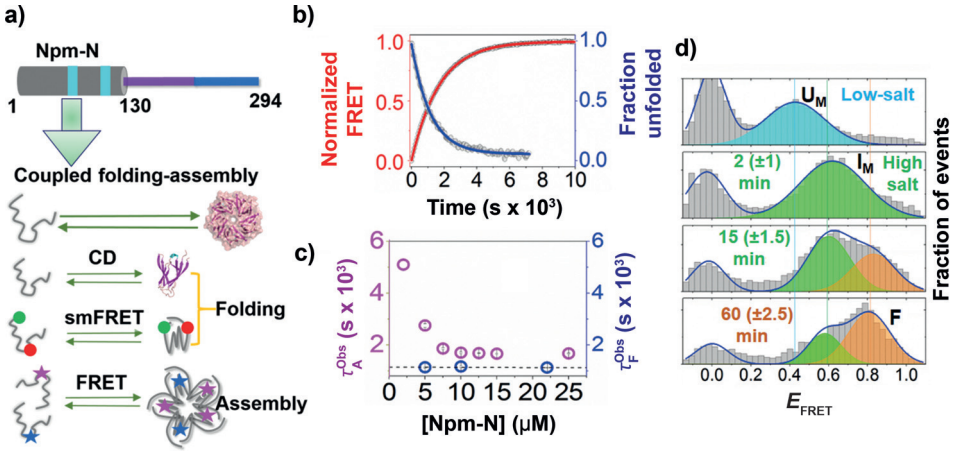

Figure 1. Folding-induced assembly of Npm-N. a) Top: Schematic illustration of the N-terminal oligomerization domain of NPM1 (Npm-N; amino acids 1–130). The cyan patches indicate two putative nuclear export signaling (NES) motifs. Bottom: Different experimental assays used to study the coupled folding and assembly kinetics of Npm-N. b) Representative folding (blue) and assembly (red) kinetic traces of Npm-N ([Npm-N] = 10 μM) at a high salt concentration (150 mM NaCl). The points are experimental data, lines are fits to appropriate models (see the Supporting Information) and yield the time constants $\tau_F = (1167 \pm 7)$ s and $\tau_A^{obs} = (1711 \pm 11)$ s. c) Concentration dependence of the folding and assembly time constants. The dotted line indicates the average value of τ_F. d) smFRET histograms showing the folding pathway of Npm-N at 150 mM NaCl. The solid lines represent fitting of the experimental data to a Gaussian model. The peak at zero is due to molecules lacking an active acceptor dye. The time values in parenthesis indicate uncertainties due to the finite data-acquisition time.

a hydroxylamine derivative of the Alexa488 dye. In the second step, the native C104 residue was labeled with the Alexa594 dye via a thiol–maleimide coupling reaction. Intramolecular smFRET experiments with Npm-N 1*/104 revealed that switching from a low to a high salt concentration resulted in a transition from the disordered monomer (FRET efficiency, $E_{FRET} \approx 0.45$; Figure 1d; see also Figure 4 in the Supporting Information) to a new, more compact state with $E_{FRET} \approx 0.60$ (Figure 1d). This transition occurs much faster than the timescales of either secondary-structure or oligomer formation (Figure 1b,c; see also Figure 5 in the Supporting Information), as measured by ensemble CD or intermolecular FRET experiments, and therefore represents a transition from U_M to a more compact but still disordered monomer (I_M). Since the net charge of Npm-N at pH 7.0 is −16,[10] charge screening by the salt is likely to be the cause of the observed collapse of the Npm-N backbone, as previously observed for other charged IDPs.[11] Our smFRET data also showed a slower process, with a new high-FRET peak ($E_{FRET} \approx 0.82$; F state; see Figure 3a in the Supporting Information) that appeared with a concomitant decrease in the I_M peak (Figure 1d; see Figure 3b in the Supporting Information), consistent with a two-state process. The time constant of this slower process is similar to that of secondary-structure formation by CD. These results together indicate a two-state transition from I_M to the folded monomer (F_M). We further validated these findings with smFRET experiments on another dual-labeled Npm-N construct, which was conventionally labeled via cysteine–maleimide coupling (see Figure 6 in the Supporting Information). Together, the single-molecule and ensemble data suggest a complex folding-induced assembly mechanism (Figure 2c) during pentamer formation at a high salt concentration, whereby the disordered monomer (U_M) first undergoes a relatively rapid collapse to form a disordered intermediate (I_M), which is then slowly converted into the folded monomer (F_M), followed by assembly into the folded pentamer (F_P; Figure 4).

We next used the same methods to study the disassembly of pentameric Npm-N at the low salt concentration (7.5 mM NaCl). Intriguingly, we observed that an alternative pathway was followed. While unfolding was monophasic (by CD, $\tau_U = (691 \pm 13)$ s; Figure 2a; see also Figures 1c and 7a in the Supporting Information), the decay of intermolecular FRET was observed to have at least three phases (Figure 2a; see also Figure 7b in the Supporting Information). The relatively fast time constant τ^1_D is comparable to the τ_U value observed by CD, whereas the other two time constants (τ^2_D and τ^3_D) were approximately 3- and 16-fold slower than τ_U (see Table 2 in the Supporting Information). Since the slowest step could be attributed to the transition to monomers, the two faster steps must correspond

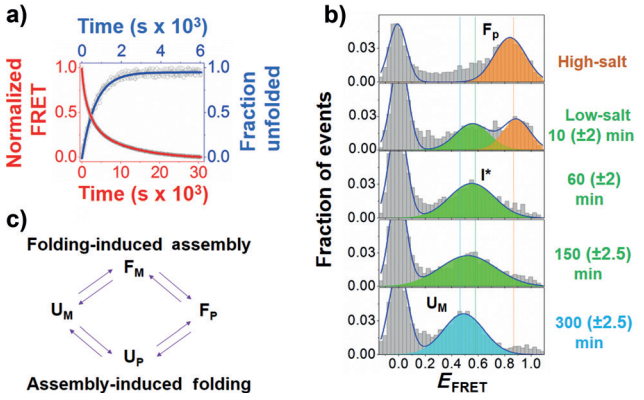

Figure 2. Unfolding-induced disassembly of Npm-N. a) Representative unfolding (blue) and disassembly (red) kinetic traces of Npm-N at a low salt concentration (7.5 mM NaCl). The points are experimental data, lines are fits to appropriate models (see the Supporting Information) and yield $\tau_U = (691 \pm 13)$ s, and $\tau^1_D = (594 \pm 20)$ s, $\tau^2_D = (2388 \pm 61)$ s, and $\tau^3_D = (11\,167 \pm 67)$ s. b) smFRET histograms showing the multistep unfolding–disassembly process. The time values in parenthesis indicate uncertainties due to the finite data-acquisition time. c) Alternative order–disorder transition pathways: The folding-induced assembly pathway is followed at high salt concentrations (Figure 1), whereas the assembly-induced folding pathway is favored at low salt concentrations (this figure).

to the formation of disordered, oligomeric states, whereby the fastest step is consistent with unfolding within pentamers (though other oligomeric species are also possible). smFRET experiments further validated this alternative transition pathway as a multistep process. Figure 2b shows that the F state initially transitioned to an intermediate state ($I^*/U_{Oligomer}$) with $E_{FRET} \approx 0.55$ on a time scale comparable to that determined for unfolding by CD measurements (Figure 2a). Subsequently, the I* state was converted relatively slowly into a somewhat lower E_{FRET} state, in agreement with the slower phases leading to U_M, as deduced from our ensemble intermolecular FRET data. Both the unfolding and disassembly processes were reasonably independent of [Npm-N], as expected for unimolecular processes (see Table 3 in the Supporting Information). Taken together, our data suggest a multistep unfolding-induced disassembly mechanism for Npm-N at low salt concentration, whereby unfolding occurs within oligomers before multistep dissociation into monomers. We can infer from the above results and the principle of microscopic reversibility[12] that an assembly-induced folding mechanism is operative for the forward reaction under these conditions (Figure 2c), though we note that this reaction occurs only to a very small extent under these conditions, which strongly favor disordered monomers.

Once we had established the mechanism of the order–disorder transition pathways of Npm-N, we next examined the effects of phosphorylation. These sites in Npm-N can be grouped as surface-exposed and buried.[1a] We first studied the effects of phosphorylation at surface-exposed sites by using the phospho-mimicking mutants T95D, S125E, and T95D/S125E,[1b] and observed significant alterations in the kinetics of order–disorder transitions for the T95D and T95D/S125E mutants, and less pronounced changes for the S125E mutant. All phosphomutants impeded the rate of assembly more than folding at the high salt concentration (see Table 2 and Figure 8a,b in the Supporting Information), thereby temporally decoupling the folding and assembly of Npm-N. Thus, the relative time that Npm-N samples the intermediate folded monomeric state (F_M) is increased in these mutants, as compared to the wild-type (WT) protein. We observed that T95D has a more dramatic effect than S125E, probably as a result of their respective locations in pentameric Npm-N.[1b,13] T95 is part of the folded core, whereas S125 is located in a flexible disordered region, relatively remote from the β-sheet core. Next, we investigated another phosphomutant, S48E, with phosphorylation at a buried site, which favors the disordered monomeric form.[1b] CD experiments indicated signatures of a random coil instead of a folded β-sheet structure (F state) for the S48E mutant at the high salt concentration (see Figure 9 in the Supporting Information), consistent with the severe thermodynamic instability of its pentameric state, as estimated previously.[1a] Remarkably, smFRET experiments revealed that even though the F_M state was not populated, the S48E mutant still formed and remained trapped in the folding intermediate (I_M state) at the high salt concentration (Figure 3a). Therefore, the effect of phosphomutation, in general, is manifested by an increase in the activation energy for the second step of the Npm-N folding reaction (I_M to F_M conversion), and more severely in the subsequent assembly process (Figure 4; see Note 2 for discussion in the Supporting Information).

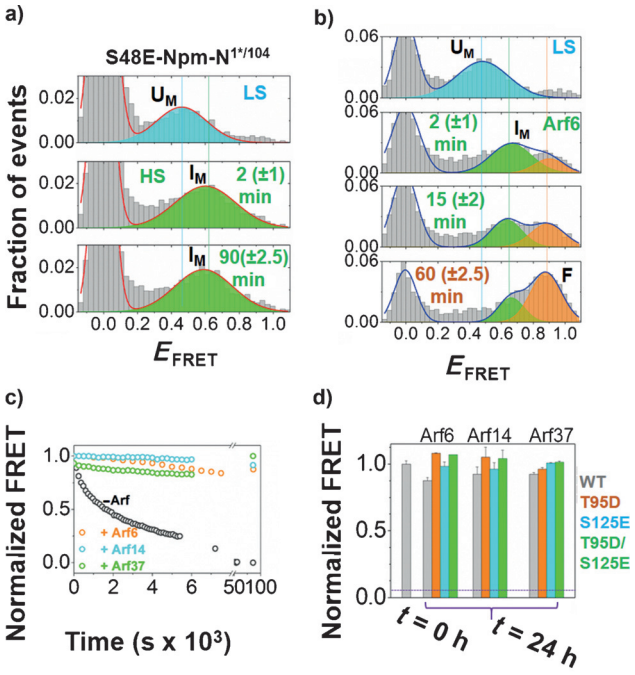

Figure 3. Effect of phosphorylation and the binding partner on the order–disorder/assembly–disassembly transitions of Npm-N. a) smFRET histograms for the phospho-mimicking variant S48E at 7.5 mM NaCl, and at two different time points after jumping to 150 mM NaCl. b) smFRET histograms for Npm-N, showing the three-state (U_M, I_M, and F_M) folding pathway induced by Arf6. c) At low salt concentration, various Arf fragments arrest Npm-N in the pentameric state, which otherwise leads to complete disassembly. d) Arf fragments counteract the unfolding–disassembly of the phosphomutants at the low salt concentration. The horizontal line represents the FRET signal observed in the absence of any Arf. The time values in parenthesis in (a) and (b) indicate uncertainties due to the finite data-acquisition time.

In the reverse reaction, although an identical pathway was followed by these mutants, the rates of unfolding and disassembly were substantially faster relative to WT Npm-N (see Table 2 and Figure 8c,d in the Supporting Information). Intriguingly, the kinetics of unfolding were more severely affected than the kinetics of disassembly, in contrast to the effects of phosphorylation on the folding–assembly pathway. The net result was a substantial increase in the lifetimes of the intermediate states ($U_{oligomer}/I^*$). Thus, the effects of phosphorylation on the unfolding–disassembly process are asymmetric, which we suggest are inherent to the alternative pathway followed under these conditions (see Note 2 in the Supporting Information for a discussion on the basis of a model).

Finally, we used linear binding motifs of the Arf tumor suppressor protein to investigate the kinetic effects of the binding partners. NPM1 is known to function in stabilizing Arf in the nucleolus by forming high-molecular-weight complexes. Binding of a six-residue R-rich fragment of Arf, corresponding to the N terminus of Arf (Arf6), mediated a disorder-to-order transition of Npm-N through a folding-induced assembly pathway (see Figure 10a,b in the Support-

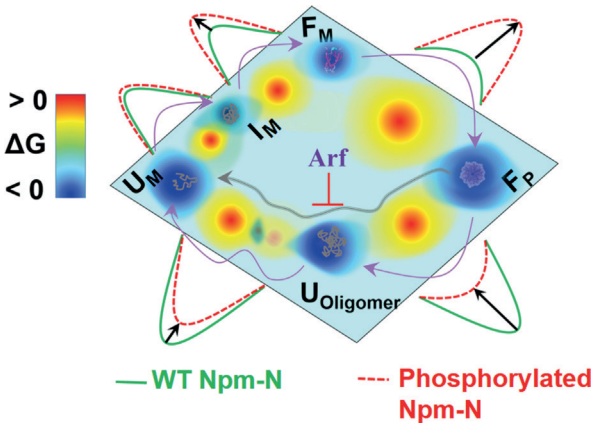

Figure 4. A 2D contour diagram showing different states of Npm-N in alternative order–disorder transition pathways. The purple arrows are guides to the eye for the direction of transition among different states under high-salt/partner-binding (folding-induced assembly) and low-salt conditions (unfolding-induced disassembly). The effect of phosphomutation in each step is shown by a relative-activation-energy barrier. Also shown is the effect of Arf in arresting Npm-N in the ordered pentamer.

ing Information). Furthermore, smFRET experiments revealed an identical three-state folding mechanism, as observed at the high salt concentration (Figure 3b), thus indicating that the I state is a conserved intermediate species in this pathway. Switching to a low salt concentration in the presence of Arf6, and more complex Arf motifs (Arf14 or Arf37), locked Npm-N in the pentameric state (Figure 3c), thus suggesting that Arf binding in the inter-subunit grooves lined by acidic A1 tracts[1b] within the Npm-N pentamer blocks the F-to-I* transition. Strikingly, when phosphomutants were used, a similar action of the Arf fragments (Figure 3d) was observed, thus indicating that partner binding can even counteract the effects of phosphorylation. These observations provide a molecular basis for the negative effect of expression of the Arf tumor suppressor, which opposes the shuttling activity of NPM1 and leads to altered intracellular localization and partial impairment of its functions.[14]

In summary, our study demonstrates that the folding and assembly of Npm-N are slow but coupled processes. We speculate that the sluggish kinetics of this important protein system could be a consequence of a relatively high energy barrier for proline *cis*/*trans* isomerization[15] (each Npm-N monomer has two *cis* proline residues in its pentameric form: P97 and P108). Our results also demonstrate tunable order–disorder transition pathways of Npm-N (Figure 4), which may provide a molecular basis for regulating the multifunctional behavior of NPM1.[4a] We speculate that the unfolding-induced disassembly mechanism can be manipulated by phosphorylation as a cellular switch for controlling the intracellular shuttling activity of NPM1.[16] Phosphorylation substantially enhances unfolding, but not disassembly, thereby decoupling these two processes. Upon unfolding, putative nuclear export signaling motifs,[17] buried within the pentameric core in Npm-N, become accessible for binding to nuclear export factors for the shuttling of oligomeric NPM1. Moreover, our proposed kinetic model suggests that the differential effects of phosphorylation are manifested by the distinct mechanistic routes that are followed at low versus high ionic strength, thus accounting for the observed asymmetry. Interestingly, partner binding can overcome the effects of phosphorylation, thus providing a molecular basis for the altered Npm-N function and localization as a result of Arf expression. Overall, our findings provide a foundation for further exploration of the mechanism of NPM1 function and disease association at the molecular and cellular levels.

Acknowledgements

This research was supported by the US NIH (grants R01 GM066833 to A.A.D. and 1R01GM115634, 2R01GM083159, 2R01CA082491 to R.W.K.), the US NSF (grant MCB1121959 to A.A.D.), the US NCI Cancer Center (support grant P30CA21765 at St. Jude Children's Research Hospital to R.W.K.), and ALSAC (grant to R.W.K.), and by the AHA (postdoctoral fellowship 15POST22520013 to P.R.B.).

Keywords: conformational landscape · coupled folding and binding · kinetics · protein folding · single-molecule FRET

How to cite: *Angew. Chem. Int. Ed.* **2016**, *55*, 1675–1679
Angew. Chem. **2016**, *128*, 1707–1711

[1] a) D. M. Mitrea, R. W. Kriwacki, *Pac. Symp. Biocomput.* **2012**, 152–163; b) D. M. Mitrea, C. R. Grace, M. Buljan, M. K. Yun, N. J. Pytel, J. Satumba, A. Nourse, C. G. Park, M. Madan Babu, S. W. White, R. W. Kriwacki, *Proc. Natl. Acad. Sci. USA* **2014**, *111*, 4466–4471.

[2] a) H. Xie, S. Vucetic, L. M. Iakoucheva, C. J. Oldfield, A. K. Dunker, Z. Obradovic, V. N. Uversky, *J. Proteome Res.* **2007**, *6*, 1917–1932; b) J. M. Rogers, V. Oleinikovas, S. L. Shammas, C. T. Wong, D. De Sancho, C. M. Baker, J. Clarke, *Proc. Natl. Acad. Sci. USA* **2014**, *111*, 15420–15425; c) U. Jakob, R. Kriwacki, V. N. Uversky, *Chem. Rev.* **2014**, *114*, 6779–6805.

[3] A. Bah, R. M. Vernon, Z. Siddiqui, M. Krzeminski, R. Muhandiram, C. Zhao, N. Sonenberg, L. E. Kay, J. D. Forman-Kay, *Nature* **2015**, *519*, 106–109.

[4] a) M. S. Lindström, *Biochem. Res. Int.* **2011**, 195209; b) D. Bertwistle, M. Sugimoto, C. J. Sherr, *Mol. Cell. Biol.* **2004**, *24*, 985–996.

[5] J. E. Herrera, J. J. Correia, A. E. Jones, M. O. Olson, *Biochemistry* **1996**, *35*, 2668–2673.

[6] a) Y. Jian, Z. Gao, J. Sun, Q. Shen, F. Feng, Y. Jing, C. Yang, *Oncogene* **2009**, *28*, 4201–4211; b) T. Enomoto, M. S. Lindström, A. Jin, H. Ke, Y. Zhang, *J. Biol. Chem.* **2006**, *281*, 18463–18472.

[7] G. Hamilton, A. G. Abraham, J. Morton, O. Sampson, D. E. Pefani, S. Khoronenkova, A. Grawenda, A. Papaspyropoulos, N. Jamieson, C. McKay, O. Sansom, G. L. Dianov, E. O'Neill, *Oncotarget* **2014**, *5*, 6142–6167.

[8] a) B. Schuler, W. A. Eaton, *Curr. Opin. Struct. Biol.* **2008**, *18*, 16–26; b) A. A. Deniz, S. Mukhopadhyay, E. A. Lemke, *J. R. Soc. Interface* **2008**, *5*, 15–45.

[9] J. M. Gilmore, R. A. Scheck, A. P. Esser-Kahn, N. S. Joshi, M. B. Francis, *Angew. Chem. Int. Ed.* **2006**, *45*, 5307–5311; *Angew. Chem.* **2006**, *118*, 5433–5437.

[10] E. Gasteiger, C. Hoogland, A. Gattiker, S. Duvaud, M. R. Wilkins, R. D. Appel, A. Bairoch in *The Proteomics Protocols*

Handbook (Ed.: J. M. Walker), Humana Press, **2005**, pp. 571 – 607.
[11] S. Müller-Späth, A. Soranno, V. Hirschfeld, H. Hofmann, S. Rüegger, L. Reymond, D. Nettels, B. Schuler, *Proc. Natl. Acad. Sci. USA* **2010**, *107*, 14609 – 14614.
[12] R. Day, V. Daggett, *J. Mol. Biol.* **2007**, *366*, 677 – 686.
[13] H. H. Lee, H. S. Kim, J. Y. Kang, B. I. Lee, J. Y. Ha, H. J. Yoon, S. O. Lim, G. Jung, S. W. Suh, *Proteins Struct. Funct. Bioinf.* **2007**, *69*, 672 – 678.
[14] a) Y. Yu, L. B. Maggi, Jr., S. N. Brady, A. J. Apicelli, M. S. Dai, H. Lu, J. D. Weber, *Mol. Cell. Biol.* **2006**, *26*, 3798 – 3809; b) S. N. Brady, Y. Yu, L. B. Maggi, Jr., J. D. Weber, *Mol. Cell. Biol.* **2004**, *24*, 9327 – 9338.
[15] W. J. Wedemeyer, E. Welker, H. A. Scheraga, *Biochemistry* **2002**, *41*, 14637 – 14644.
[16] a) L. B. Maggi, Jr., M. Kuchenruether, D. Y. Dadey, R. M. Schwope, S. Grisendi, R. R. Townsend, P. P. Pandolfi, J. D. Weber, *Mol. Cell. Biol.* **2008**, *28*, 7050 – 7065; b) R. A. Borer, C. F. Lehner, H. M. Eppenberger, E. A. Nigg, *Cell* **1989**, *56*, 379 – 390.
[17] K. Hingorani, A. Szebeni, M. O. Olson, *J. Biol. Chem.* **2000**, *275*, 24451 – 24457.

Received: August 18, 2015
Revised: November 2, 2015
Published online: December 17, 2015

